Two routes to hydrogen evolution for a Co-polypyridyl complex with two open sites

Electronic Structure

OPEN ACCESS

PAPER

Two routes to hydrogen evolution for a Co-polypyridyl complex with two open sites

Liqin Xue Toro[1], Sofia Kiriakidi[2], Anders Thapper[1], Sascha Ott[1] and Marcus Lundberg[1,*]

[1] Department of Chemistry—Ångström Laboratory, Uppsala University, Box 538, SE-751 21, Uppsala, Sweden
[2] University of Vigo, Department of Organic Chemistry, Campus Lagoas-Marcosende, Vigo, Galicia, ES 36310, Spain
* Author to whom any correspondence should be addressed.

E-mail: marcus.lundberg@kemi.uu.se

RECEIVED
19 March 2022

REVISED
26 May 2022

ACCEPTED FOR PUBLICATION
23 June 2022

PUBLISHED
8 July 2022

Keywords: proton reduction, electrocatalysis, density-functional theory, metal hydride, polypyridyl ligand, reaction mechanism

Supplementary material for this article is available online

Abstract

Cobalt polypyridyl complexes efficiently catalyze hydrogen evolution in aqueous media and exhibit high stability under reducing conditions. Their stability and activity can be tuned through electronic and steric considerations, but the rationalization of these effects requires detailed mechanistic understanding. As an example, tetradentate ligands with two non-permanently occupied coordination sites show higher activity with these sites in cis compared to trans configuration. Here reaction mechanisms of the Co-polypyridyl complex $[Co^{II}(bpma)Cl_2]$ (bpma = bipyridinylmethyl-pyridinylmethyl-methyl-amine) have been studied using hybrid density-functional theory. This complex has two exchangeable cis sites, and provides a flexible ligand environment with both pyridyl and amine coordination. Two main pathways with low barriers are found. One pathway, which includes both open sites, is hydrogen evolution from a Co^{II}-H intermediate with a water ligand as the proton donor. In the second pathway H–H bond formation occurs between the hydride and the protonated bpma ligand, with one open site acting as a spectator. The two pathways have similar barriers at higher pH, while the latter becomes more dominant at lower pH. The calculations consider a large number of interconnected variables; protonation sites, isomers, spin multiplicities, and the identities of the open binding sites, as well as their combinations, thus exploring many simultaneous dimensions within each pathway. The results highlight the effects of having two open cis-coordination sites and how their relative binding affinities change during the reaction pathway. They also illustrate why Co^{II}-H intermediates are more active than Co^{III}-H ones, and why pyridyl protonation gives lower reaction barriers than amine protonation.

1. Introduction

Conversion of solar energy to chemical energy has attracted great interest in recent decades as alternatives to fossile fuels. Hydrogen is a power-dense fuel that can be generated from photochemical or electrocatalytic reduction of water. For large-scale applications, it is desirable to find catalysts based on earth-abundant first-row transition metals [1–7], e.g., iron [8], cobalt [9–14], or nickel [15, 16]. Here the focus will be on molecular cobalt catalysts. Molecular complexes combine high stability and excellent catalytic activity with a possibility to tune properties through systematic ligand modifications [17]. There is also considerable interest in using Co complexes in different types of hybrid and supramolecular systems and electrodes to combine the strengths of homogeneous and heterogeneous catalysis [18–23].

Two main classes of Co-based complexes show high activity for proton reduction, hydridocobaloximes and polypyridyl complexes, see figure 1. Cobaloximes were shown to evolve hydrogen already back in 1971 [24], and have together with the related diamine–dioxime complexes, been investigated in detail from both

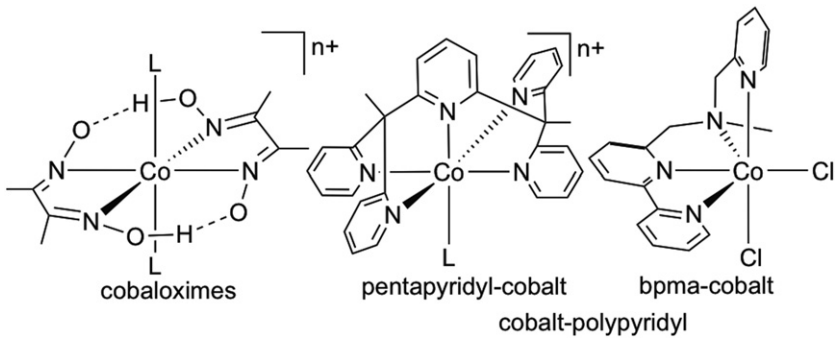

Figure 1. Examples of structures for cobaloximes and cobalt-polypyridyl complexes (L = solvent (H_2O, CH_3CN, DMF), pyridine, Cl^-, ...), including the the bpma-cobalt (bpma = bipyridinylmethyl-pyridinylmethyl-methyl-amine) complex studied here.

experimental [25–28] and theoretical [29–32] perspectives. Comprehensive reviews of hydrogen evolution from water are also available [7, 33–35]. The other class is cobalt-polypyridyl complexes utilizing multidentate polypyridyl ligands, with an early example from 1981 being $[Co(bpy)_3]^{2+}$ (bpy = 2,2'-bipyridine) [36, 37]. Polypyridyl complexes are generally more stable than cobaloximes in reductive and acidic conditions, and the π-backbonding from the pyridyls to cobalt can stabilize reduced intermediates [5, 11, 17, 38]. In some cases, pyridyls might also be directly involved in the reaction as redox *non innocent* ligands [39, 40].

From the first Co-polypyridyl catalysts [41, 42], the latest decade has shown significant progress in developing new complexes of this class [17]. There now exists a number of variations with regard to coordination number, ligand identity, substituent groups, and external ligands. A key development compared to the early bipyridine complexes has been to increase the denticity of the ligands to achieve increased stability [7]. In 2011 Chang and co-workers described a highly active pentapyridyl-cobalt complex, as shown in figure 1, as an electrocatalyst for proton reduction in aqueous buffer [42]. Pentapyridyl-cobalt complexes for electrochemical hydrogen evolution from neutral water were developed by Singh *et al* [43] and Zhang *et al* [44], respectively. Photoinduced hydrogen evolution has been reported as well [17, 45–51].

Reducing the denticity of the polypyridyl ligand from five to four gives two exchangeable coordination sites [41]. These tetradentate complexes can actually be related to $[Co(bpy)_3]^{2+}$, for which the proposed mechanism of activation is de-coordination of a bpy ligand to form $[Co(bpy)_2(H_2O)_2]^{2+}$ [5]. The presence of two labile coordination sites opens up reaction channels that involve both these sites, and one the question is whether such channels play important roles. In studies of photocatalytic hydrogen generation, pyridyl ligands that enforce two vacant sites in cis position show higher activity compared those that enforce sites in trans position [5, 45]. A large number of such tetradentate complexes have now been synthesized and reported as proton reduction catalysts [41, 45, 52–59].

Here we report a theoretical study of the mechanism for proton reduction for the $[Co^{II}(bpma)Cl_2]$ (bpma = bipyridinylmethyl-pyridinylmethyl-methyl-amine) complex, see figure 1 [52]. The cyclic voltammogram (CV) in aqueous solution shows catalytic hydrogen evolution at −1.4 V (vs Ag/AgCl) for pH values below 10. A putative cobalt-hydride intermediate could be identified in the oxidation wave of the CV. Among the tetradentate complexes, the Co-bpma complex is of special interest as one of the pyridyls has been replaced with an amine to create a flexible tetradentate polypyridyl ligand, thus opening up for even more mechanistic alternatives.

Understanding the reaction pathway is necessary for rational design of more stable and efficient catalysts. This is highlighted by several studies that show how small changes in the ligand affect catalytic performance, although sometimes with seemingly contradictory results [13, 40, 45, 46, 53, 55, 59–64]. As an example, adding an electron withdrawing $-CF_3$ group in $Co(bpy)_2PyMe$ depresses catalytic activity [46], while it increases activity in Co-pentapyridyl complexes [13]. The effects thus depend on substituent position [55], and to rationalize these effects requires detailed mechanistic insights [59].

Initially proposed for diimine–dioxime catalysts by the Eisenberg group [65], an initial reduction from Co^{II} to Co^{I}, can lead to the formation of a Co^{II}-H hydride species, which then can form $Co^{II}(H_2)$ through a second protonation from a general acid [31, 32]. Hydrogen evolution can also occur via a bridge-protonation pathway [29]. Here the second protonation occurs at the ligand, giving the active species Co^{II}-H(LH) (L = ligand), and the H–H bond is formed between the hydride and the ligand proton [61, 66]. Similar ligand-protonation mechanisms have been proposed for hydrogenase enzymes [67], and functional models thereof [68–71].

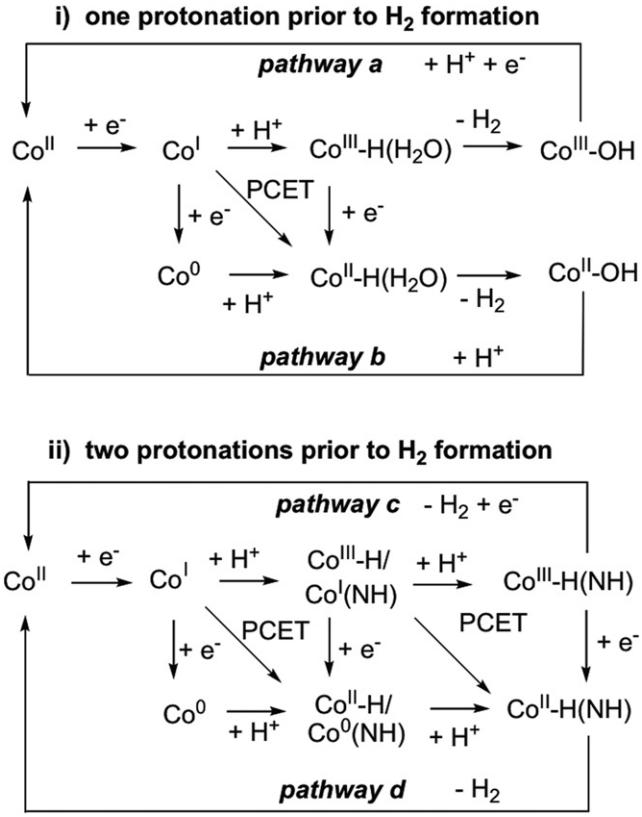

Figure 2. Proposed unimolecular mechanisms for proton reduction. Metal ligands are only shown when directly involved in the reaction. This includes H_2O in pathways **a** and **b**, as well as the pyridyl/amine nitrogen in the bpma ligand (N) in pathways **c** and **d**.

Potential hydrogen evolution pathways for the $[Co^{II}(bpma)Cl_2]$ catalyst are depicted in figure 2. They are classified according to the number of protonation steps prior to H–H bond formation, with (i) a single protonation and (ii) two protonations. All pathways start with the reduction of Co^{II} to Co^{I}, an intermediate that has been characterized in several systems [9, 38, 50, 72–74]. In (i), generation of a cobalt hydride with a water ligand present in the *cis* position, enables direct formation of H_2 in a reaction between the hydride and a water proton. The hydride can be on either Co^{III} or Co^{II}, giving pathways **a** and **b**. If instead the complex is protonated twice before H_2 formation (ii), the key intermediate becomes Co-H(NH). This gives pathways **c** and **d** where the reactions occur between the hydrides and the protonated ligand.

Density-functional theory has been frequently used to analyze mechanisms of cobalt pentapyridyl complexes [38–40, 43, 46, 54, 59, 61–63, 66, 73, 75, 76]. Herein, we present a detailed study of the different electrocatalytic proton reduction pathways in figure 2 using the B3LYP-D3 [77, 78] functional with 15% HF exact exchange (B3LYP*) [79]. B3LYP* provides a good balance for spin-state energetics and reaction energies, and has been widely used to study transition-metal catalysts, e.g., by the Siegbahn group [80]. However, the inherent sensitivity of the results to the choice of functional must be considered. Fortunately, the functional sensitivity of key steps for cobalt-based catalysts have already been explored through a comparison between B3LYP and the local BP86 functional [29]. Reaction steps that include a significant change in spin multiplicity show the strongest sensitivity. As an example, the relative stability of different hydride species depends strongly on the method. With local functionals, the low-spin Co^{III}-H is significantly stabilized compared to the high-spin Co^{II}-H [29, 61, 63]. The B3LYP* functional was optimized specifically to reproduce spin-state energetics of transition-metal complexes, and is thus expected to give reasonable results for the most sensitive reaction steps. Other properties such as reaction barriers are much less sensitive to choice of functional, making it possible to compare results for related mechanisms [29].

Here results will be presented for all reaction pathways in figure 2. Bimolecular mechanisms including two Co-H complexes have not been considered. Experimentally, the possibilities of reactions between two Co-H complexes have been evaluated in reference [72]. They could not rule out contributions from a bimolecular pathway, but established an upper limit of 5% with regards to hydrogen production. Bimolecular reactions between two polypyridyl complexes were modeled in reference [76], for both Co^{III}-H and Co^{II}-H. These reactions had unfavorable reaction energies compared to reactions involving a single Co-hydride, and were

therefore ruled out. Although these calculations were performed for pentapyridyl complexes, the clear energy differences means that the bimolecular reactions should be unfavorable also for the Co(bpma) complex. Another modeling decision is that for pathways **a** and **b**, only ligand water is considered as proton donor. This is due to an expected increase in acidity upon metal binding. An intramolecular reaction should also be entropically more favorable than an intermolecular reaction with bulk water.

For each pathway, several alternative mechanisms will be considered that arise from the presence of two open cis sites. One such variation includes the identities of the ligands of these sites, including different isomers. As the binding affinity of external ligands in polypyridyl complexes varies with oxidation state [81], these variations will be explored along the full reaction pathways, thus giving a unique mapping of possible reactions for this class of flexible cobalt catalysts. The differences between amine and pyridyl ligand protonation will also be explored, as well as changes in spin multiplicity along the reaction pathways.

2. Computational details

All the calculations were performed with Gaussian 09 [82] using the B3LYP [77] functional with 15% HF exact exchange (B3LYP*) [79]. Molecular geometries were optimized using the SMD solvation model (solvent = water), unless otherwise stated [83], and the cc-pVDZ basis set [84]. Self-consistent field and geometry optimizations are performed using the default algorithms and convergence criteria in Gaussian 09. Frequency calculations at the same level of theory were performed to characterize stationary points and provide thermal corrections to free energies at 298.15 K. Transition states (TS) have been located by explicitly calculating the force constants for potential TS structures obtained from constrained optimizations with frozen reaction coordinates. These force constants are then used to guide the subsequent full TS optimizations. Calculations of intrinsic reaction coordinates [85] in vicinity of the TS were performed to confirm that they connect relevant minima. Minimum energy crossing points between different spin multiplicities have not been optimized, but are believed to be located close to the stationary point with the highest relative energy [86, 87].

Cartesian coordinates of all relevant complexes are given in the supplementary information (https://stacks.iop.org/EST/4/034002/mmedia) (SI). Calculations give Co–N bond lengths that are approximately 0.1 Å longer than those determined by x-ray diffraction, see figure SI-1. Longer Co–N bond lengths could indicate a slight preference for ligand dissociation, but these errors are not believed to be significant.

Electronic energies were corrected by performing single-point calculations with the cc-pVTZ basis set [88]. Grimme's dispersion corrections were applied using the B3LYP-D3 parameters as there are no B3LYP*-D3 version available [78]. Absolute energies of all relevant complexes are given together with the Cartesian coordinates in the SI.

The free energy change associated with compressing an ideal gas from the molar volume of 24.5 l to 1 l at room temperature is 1.9 kcal mol^{-1} (RT ln(24.5)). Hence, the solvation corrected Gibbs free energies were defined as $G = E_{(\text{cc-pVTZ})} + E^{(\text{thermal correction to Gibbs free energy})}{}_{(\text{cc-pVDZ})} + E_{(\text{dispersion correction})} + 1.9$. Pure water has a concentration of 55.6 M and converting from 1 M gives an additional free-energy correction for water of 2.4 kcal mol^{-1} (RT ln(55.6)). For the exchange reactions with Cl^- a correction of −6.5 kcal mol^{-1} was applied as the stability of solvated chloride is underestimated by the SMD solvation model [83].

For calculation of free energies of protonation reactions, a value of −264.0 kcal mol^{-1} was used for the absolute solvation energy of a proton in aqueous solution [89, 90], with −6.3 kcal mol^{-1} as a correction for the free energy of a gas phase proton from the Sackur–Tetrode equation [91]. Reaction energies were calculated for pH = 10, not pH = 0, and the correction for the reduced concentration of proton was −13.6 kcal mol^{-1} using pH*(−1.36) kcal mol^{-1}. This gave −283.9 kcal mol^{-1} (=−264.0−6.3−13.6 kcal mol^{-1}) as the solvated Gibbs free energy of a proton in water at pH = 10.

Redox potentials are given in V vs Ag/AgCl for easy comparison with experimental results. To calculate these half potentials, an electron affinity of 103.8 kcal mol^{-1} is used. This corresponds to an absolute potential of −4.503 V = (−0.222−4.281 V), where −0.222 V is the $E_{1/2}$ of Ag/AgCl vs. the standard hydrogen electrode (SHE) in aqueous solution [92], and −4.281 V is absolute SHE potential in water [93]. Unless otherwise stated, relative reaction energies are calculated for an applied potential of $E = -1.37$ V, corresponding to the reversible wave in the CV. Calculations of absolute pKa values and redox potentials of transition metal complexes often show significant errors, up to 10 pKa units and 0.5 eV [94–98]. This makes it difficult to accurately estimate the relative energies of species with different charge or protonation states. Trends between complexes can be reproduced with higher accuracy [94–98].

The present combination of functional and basis set was tested for the $Fc^{+/0}$ redox couple and the CV of $[Co^{II}(bpma)Cl_2]$ in CH_3CN. The $Fc^{+/0}$ calculations had an error of only 0.03 eV (see table SI-1 for details). The best results for the redox events in the CV of $[Co^{II}(bpma)Cl_2]$ were obtained by assuming that one Cl^- is lost during reduction, which gave absolute errors of 0.4 eV and relative errors of less than 0.2 eV (see table SI-2).

The natural bond orbital (NBO) program [99], as implemented in Gaussian 09, was used to obtain natural populations of atoms [100]. The charge populations correspond to the number of elementary charges, i.e., a free electron corresponds to a value of −1. The spin populations correspond to the number of unpaired electrons, i.e., a free electron has a value of 1.

3. Results

Throughout the text, complexes are labeled by numbers for convenience. Prefixes **RE** in labels stands for a reduction of the species by one electron, the suffixes **Cl** and **v** stands for Cl bound or vacant coordinate site respectively, and prime (′) is used to distinguish between isomers and protonation sites. The spin multiplicities are given after the labels. The energies of all species are given relative $[Co^{II}(bpma)Cl_2]$.

3.1. Co^{II} species in acetonitrile and water

The starting point for the calculations is the $[Co^{II}(bpma)\ Cl_2]$ complex (**1**). It is generally believed that anionic ligands readily exchange in aqueous solution [54, 101]. Dissolving **1** in water leads to changes in the electronic absorption spectrum, and it is believed that at least one Cl^- ligand is replaced by solvent molecules [52]. This exchange is also a requirement for all mechanisms previously mentioned. Addition of a silver salt to the aqueous solution led to further changes in the absorption spectrum, suggesting that some Cl^- bound species could be present at thermodynamic equilibrium.

In the calculations, the exchange of two Cl^- with water to get six-coordinated $[Co^{II}(bpma)(H_2O)_2]^{2+}$ (**2**) is favorable (−6.5 kcal mol^{-1}) but the energy is similar for a species with one Cl^- still bound (**2-Cl**) (−4.9 kcal mol^{-1}). Even five-coordinated structures (**3**) are only a few kcal mol^{-1} higher in energy see figure SI-2. Electron paramagnetic resonance measurements in water show that the Co^{II} complex is in a high-spin (quartet) state [52]. In **2** this state is favored by 6.5 kcal mol^{-1} relative to the doublet. Cl^- is a weaker ligand than H_2O in the spectrochemical series and all other Co^{II} complexes are also predicted to have high-spin ground states. Relative spin-state energetics of all relevant species are shown in table SI-3.

3.2. Reduction of Co^{II} to Co^{I}

The CV of the Co(bpma) complex shows a reversible redox wave around −1.4 V, which was assigned to a reduction from Co^{II} to Co^{I}. After one-electron reduction, the lowest Co^{I} species is predicted to be a five-coordinated species (**RE-3**) with an open site for hydride formation. Starting from the most stable reactant $[Co^{II}(bpma)(H_2O)_2]^{2+}$ the calculated reduction potential for the reaction (**2** + e^- → **RE-3**) is −1.44 V vs Ag/AgCl in fortuitously good agreement with experiment, see figure 3. Other structures with alternative ligand configurations are relatively close in energy, see figure SI-3, which means that they could be reached with similar potentials. From Co^{I} the reaction pathways diverge, depending on the order, number, and location of protonation and redox events, see figure 1. Further reduction to a formal Co^0 species would occur at a very low reduction potential (−2.08 V), see figure 3, and is not considered further. The next step in the reaction must therefore include a protonation.

3.3. Cobalt hydride reacting with water ligand (pathways a and b)

Starting from the five-coordinate **RE-3**, protonation of the Co^{I} metal center would lead to generation of $[Co^{III}H(bpma)(H_2O)]^{2+}$ (**4**) as proposed in reference [52], see figure 3. The calculations suggest that Co^{I} is not a strong base and at pH 10 formation of the Co^{III}-H species is uphill by 8.8 kcal mol^{-1}. Formation of **4** directly from Co^{II} in a proton-coupled electron transfer (PCET) process has a potential of −1.82 V, reflecting the low proton affinity in this step. Generating the hydride is more facile if the oxidation state of Co is lower. The Co^{II}-hydride $[Co^{II}H(bpma)(H_2O)]^+$ **RE-4** can be directly generated from Co^{I} through a PCET process (**RE-3** + e^- + H^+ → **RE-4**) at −1.31 V, see figure 3. This is a more positive potential than the Co^{II}/Co^{I} reduction step, which suggests that this is a viable route. In some systems, hydride generation has been proposed as a rate-limiting step [14, 59], but as it is the same in all pathways it has not been explicitly modeled here.

Both Co^{III}-H and Co^{II}-H can in principle generate hydrogen together with a suitable proton donor. In pathways **a** and **b**, the proton donor is the water ligand bound to the metal ion. Calculations of the pKa of the water ligand, see figure SI-4, indicate that the water ligand remains protonated even at relatively high pH, and should thus be available to serve as a proton donor. Although the Co^{III}-H species **4** appears less stable, it could be relevant if it is sufficiently reactive. However, pathway **a** with H–H bond formation from Co^{III}-H and water (**TS1**) to form $[Co^{III}(OH)(bpma)]^{2+}$ + H_2 (**5**) has a total energy barrier of 36.7 kcal mol^{-1} relative to **2,** see figure 4. The high reaction barrier excludes pathway **a**. The situation is different for the Co^{II}-H pathway **b**. Here the barrier height is only 9.3 kcal mol^{-1} (**TS2′**) see figure 5, which would give a rapid reaction. After passing the barrier, a Co^{II}-hydroxo species $[Co^{II}(OH)(bpma)]^+$ (**6**) is formed, which can then be protonated and re-bind water to complete the catalytic cycle.

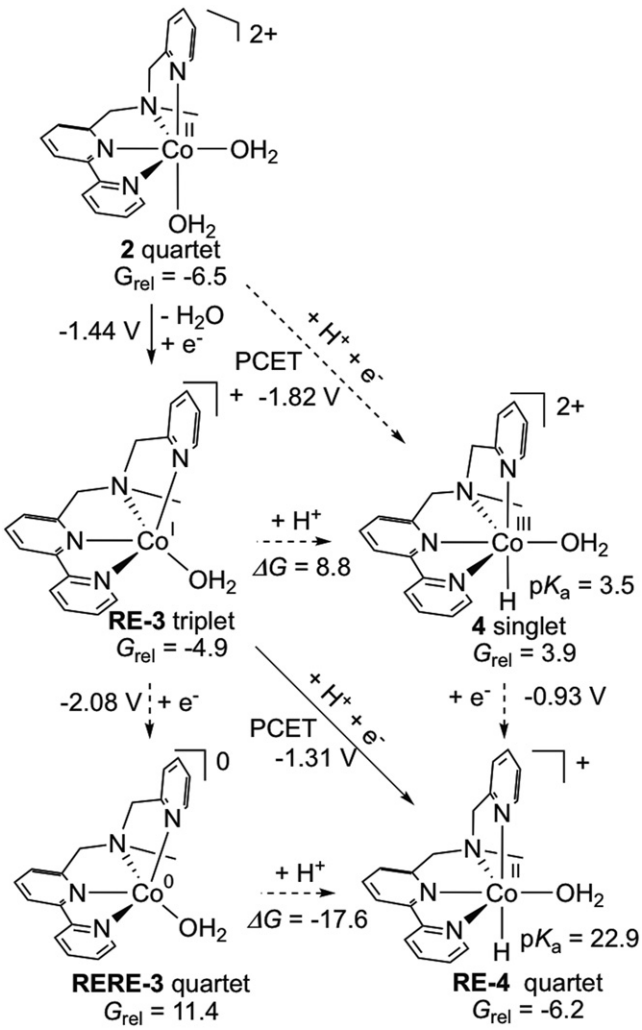

Figure 3. Relative energies and potentials for generation of cobalt-hydride species. Redox potentials are in V vs Ag/AgCl, and relative Gibbs free energies (G_{rel}) in kcal mol^{-1} at pH = 10 with [Co^{II}(bpma)Cl_2] **1** as the zero of energy. Solid arrows indicate preferable pathways. The prefix **RERE** denotes a doubly reduced species.

In both pathways the hydride can be either in the axial or equatorial position. Focusing on the more favorable pathway **b**, the two sites have similar energies (ΔG = 0.3 kcal mol^{-1}) in the Co^{II}-H intermediate (**RE-4/RE-4′**), but the equatorial isomer gives the lowest barrier (**TS2/TS2′**), see figure 5. Among possible spin multiplicities, the quartet is predicted to be more stable than the doublet, although the difference is small (<1 kcal mol^{-1}) for the Co^{II}-H species and the proceeding TS, see table SI-3.

3.4. Cobalt hydride reacting with protonated bpma ligand (pathways c and d)

As previously proposed for the cobaloximes, alternative pathways include reactions with a protonated ligand [29]. Again starting from the Co^{I} species **RE-3**, one possibility is to directly protonate either a pyridyl that decoordinates and become dangling (**7**) or the amine (**7′**) to form a Co^{I}(NH) species [Co^{I}(bpmaH)(H_2O)]$^{2+}$, see figure SI-5 [40]. This requires at least 11.3 kcal mol^{-1} compared to **RE-3**, which makes them less stable than Co^{III}-H (**4**) by 2.5 kcal mol^{-1} or more. Pathway **c** can be discarded because generating the corresponding hydride Co^{III}-H(NH) [Co^{III}H(bpmaH)(H_2O)]$^{3+}$ (**8**) is uphill by more than 30 kcal mol^{-1} compared to [Co^{II}(bpma)$(H_2O)_2$]$^{2+}$ (**2**).

As expected, forming a hydride with a protonated ligand is significantly easier for the one-electron reduced species (pathway **d**). The Co^{II}-hydride **RE-4**, which was the reactant in the hydride–water process, can be protonated at the pyridyl to generate Co^{II}-H(NH) (**RE-8**). This process is uphill by 8.3 kcal mol^{-1}, see figure 6, which would make the protonated form a minority species at the experimental pH.

The Co^{II}-H(NH) species (**RE-8**) could in theory go through a similar hydride–water mechanism as in pathway **b**, with the protonated ligand as spectator. However, the relative instability of Co^{II}-H(NH) leads to a high barrier (26.9 kcal mol^{-1}) for **TS3**, see figure SI-6, which makes this unlikely. For completeness, that

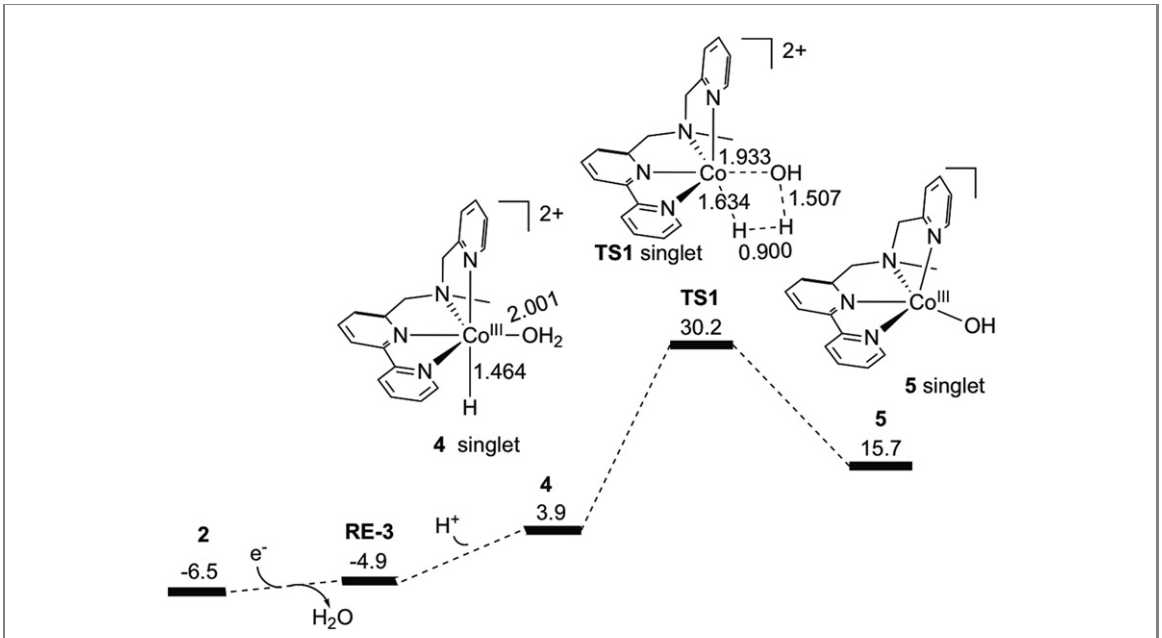

Figure 4. Free energy profile for pathway **a**, the reaction between a Co^{III}-hydride and a water ligand. Energies (in kcal mol^{-1}) are given at pH = 10 with $[Co^{II}(bpma)Cl_2]$ **1** as the zero of energy. Selected bond distances are given in Å.

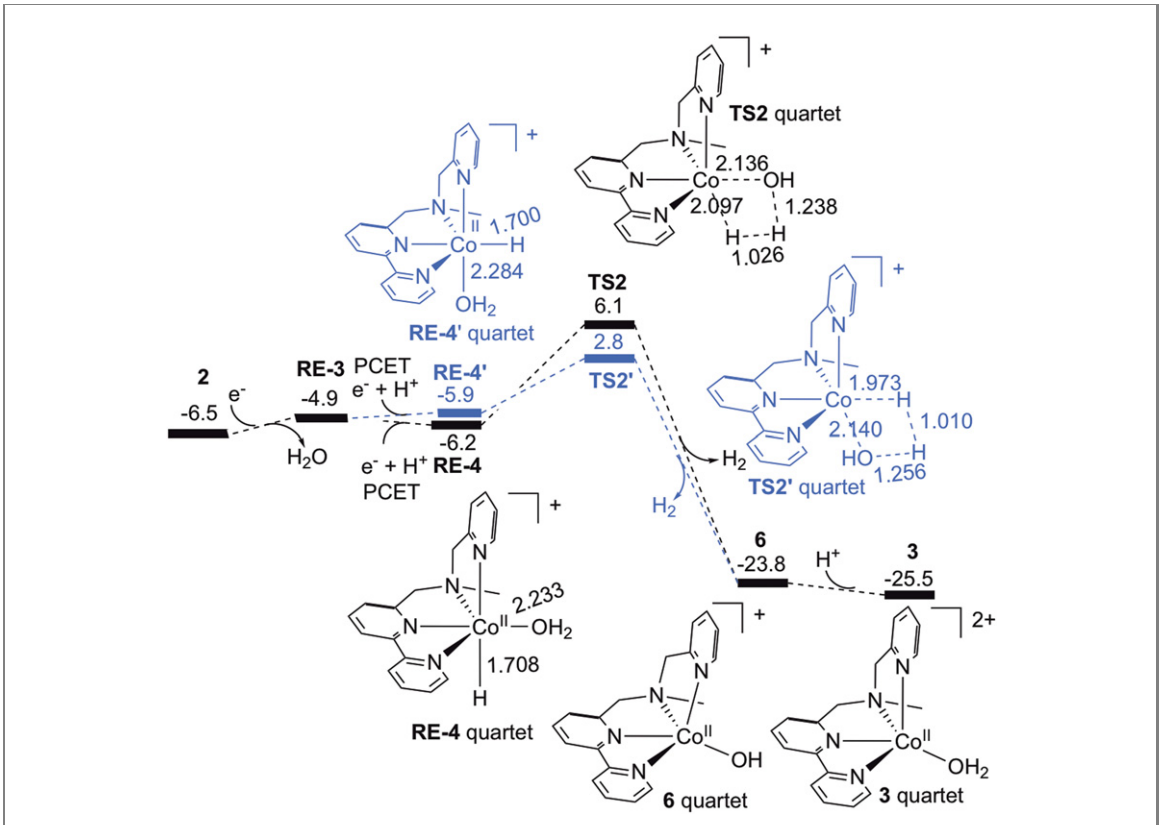

Figure 5. Free energy profile for pathway **b**, the reaction between a Co^{II}-hydride and a water ligand. Energies (in kcal mol^{-1}) are given at pH = 10 with $[Co^{II}(bpma)Cl_2]$ **1** as the zero of energy. Selected bond distances are given in Å.

reaction would then proceed through additional barriers (**TS4/TS5**) and intermediates (**9/10**) for H_2 release and ligand deprotonation before completing the catalytic cycle.

Alternatively, focusing on the reaction between the hydride and the protonated ligand, the TS for H_2 formation (**TS6**) has a barrier of only 0.8 kcal mol^{-1} relative to Co^{II}-H(NH) (**RE-8**), see figure 6. Together with the energy required to protonate the ligand, the total barrier for pathway **d** is 9.4 kcal mol^{-1}. This is comparable to the barrier for the hydride–water reaction (pathway **b** with 9.3 kcal mol^{-1}). The product is the Co^{II} species $[Co^{II}(bpma)(H_2O)]^{2+}$ **3**, which can re-bind water and serve as a starting point for a new catalytic cycle.

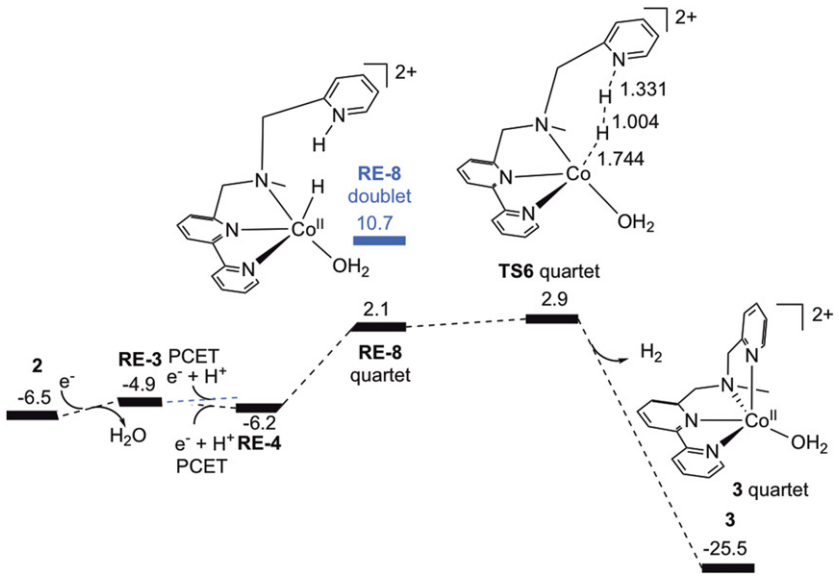

Figure 6. Free energy profile in kcal mol^{-1} calculated for reaction between protonated pyridyl ligand and Co^{II}-hydride (pathway **d**) with [Co^{II}(bpma)Cl$_2$] **1** as the zero of energy. Energies and structures with quartet state or doublet states are in black and in blue, respectively. Selected bond distances are given in Å.

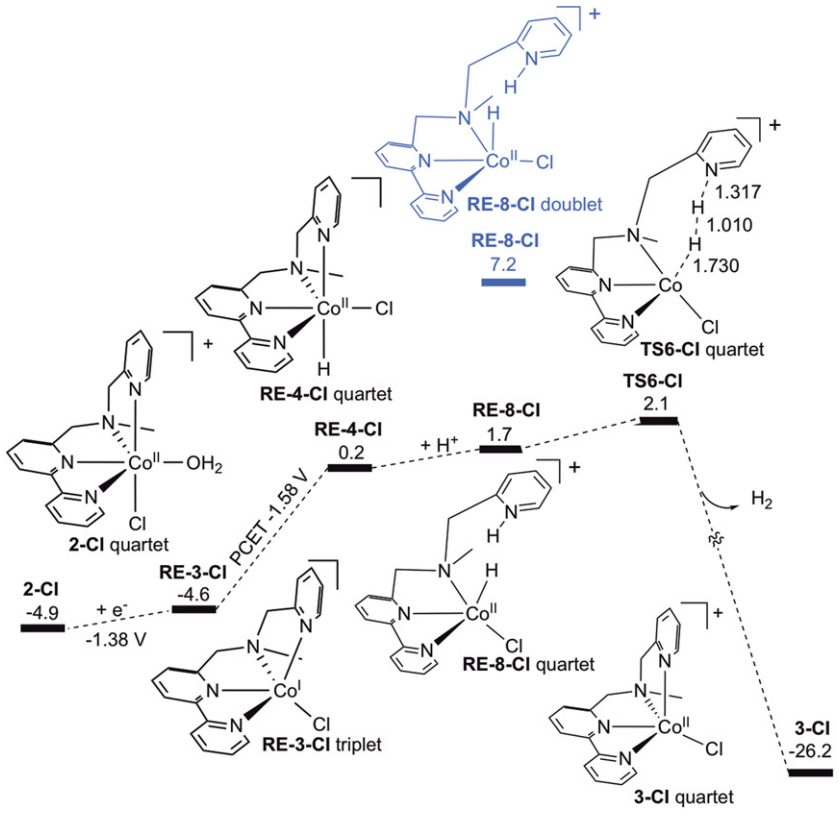

Figure 7. Free energy profile for the reaction between protonated ligand and Co^{II}-hydride with Cl bound to Co, starting from [Co^{II}(bpma)Cl(H$_2$O)]$^+$ **2-Cl**. [Co^{II}(bpma)Cl$_2$] **1** is used as the zero of energy. Selected bond distances are given in Å.

For pathway **d**, there exist a large number of different variations. First of all, protonation can occur at either the pyridyl or the amine. Protonation of a dangling pyridyl is more favorable throughout. The amine-protonated Co^{II}-H(NH) (**RE-8′**) is only 1.1 kcal mol^{-1} higher in energy than **RE-8**, but the corresponding transition state (**TS6′**) is 5.1 kcal mol^{-1} less favorable than **TS6**, see figure SI-7.

As the reaction between the hydride and the protonated bpma ligand does not involve the sixth ligand position, this reaction path remains open even if not all chloride ligands exchange in water. Starting from the

$[Co^{II}(bpma)Cl(H_2O)]^+$ complex (**2-Cl**), this can be reduced to Co^I at −1.38 V, and further undergo a PCET and a second protonation to form the doubly-protonated $[Co^{II}H(bpmaH)Cl]^{2+}$ (**RE-8-Cl**) 6.6 kcal mol^{-1} higher than the starting point, see figure 7. From here the barrier for H–H bond formation (**TS-6-Cl**) is only 0.4 kcal mol^{-1}, which gives a total barrier relative to **2-Cl** of 7.1 kcal mol^{-1}. If Cl^- stays bound during the entire reaction, the barrier for H–H bond formation with a Cl^- ligand as spectator is slightly lower than the reaction with a water ligand. The corresponding barrier with the protonated amine (**TS-6-Cl′**) is slightly more unfavorable, with a total barrier of 9.1 kcal mol^{-1}, see figure SI-8.

Similarly, pathway **d** can proceed with a vacant sixth site. The five-coordinated Co^{II}-H species (**RE-4-v**) is only slightly less stable (+1.8 kcal mol^{-1}) compared to the same species with a water ligand (**RE-4**). However, protonation of that hydride to form a five-coordinated Co^{II}-H(NH) (**RE-8-v**) is uphill by 7.6 kcal mol^{-1}, which leads to a total barrier of 13.3 kcal mol^{-1}, see figure SI-9. This is significantly higher than with a bound Cl^- or H_2O ligand.

Finally, after considering different hydride mechanisms, it should be noted that a protonated ligand could in principle form a H–H bond with proton from water in the Co^{II}-H(NH) species **RE-8**. However, no such TS could be located. This is understandable because of the mutual repulsion. Further reduction to a formal Co^0(NH) (**RE-7**) has a very low potential −2.15 V, hence non-hydride mechanisms can be discarded.

4. Discussion

Results have been presented for several different reaction pathways for hydrogen formation from the complex $[Co^{II}(bpma)Cl_2]$. For each of them several alternatives have been considered with respect to the ligands at the two cis sites, their isomers, the bpma ligand protonation sites and possible spin multiplicities of all species. When considered together, this gives rise to a very large number of mechanisms. Here the main differences between them will be discussed. When analyzing the results, the findings should be related to the limitations of the method. Comparisons between species with significant differences in the number of unpaired electrons show strong functional sensitivity [29]. Another challenge is to correctly calculate the energies of single protonation and reduction steps because of the large environmental effects for changes in system charge. The calculations of PCET steps should be more accurate, assuming that errors for consecutive reductions and protonations partly cancel. Barrier heights relative to the preceding intermediates should also be comparable between pathways.

4.1. Comparing cobalt(III) and cobalt(II) hydrides

The calculations clearly show that formation of a cobalt-hydride intermediate is a key step, but that only the Co^{II}-hydride gives a sufficiently low barrier. This general conclusion is in good agreement with other DFT studies, and largely independent of the choice of functional [29, 32, 43, 54, 59, 61, 73, 75, 102, 103]. This is in apparent contradiction to the original assignment of the pH-dependent oxidation wave that appears at high pH as coming from a Co^{III}-H species [52].

In the present calculations, there are two factors that favor H–H bond formation from Co^{II}-H over Co^{III}-H, relative hydride stability and relative barrier heights. First, Co^{II}-H is predicted to be more stable at the applied potential (by 8.8 kcal mol^{-1}). However, as mentioned previously the relative stability of the two hydride species is sensitive to the choice of functional. The hybrid B3LYP functional gives unstable Co^{III}-H species [63], while local functionals like BP86, M06-L, and PBE favor Co^{III}-H [66, 75], with deviations between methods of 10 kcal mol^{-1} [29]. An important reason for the functional sensitivity is that Co^{III}-H is a low-spin (singlet) species, while Co^{II}-H is predicted to be high spin (quartet). As HF exchange favors unpaired electrons, this is directly reflected in relative hydride stability. B3LYP* correctly predicted the quartet state of $[Co^{II}(bpma)(H_2O)_2]^{2+}$ (**2**), with an energy difference is 6.5 kcal mol^{-1} relative to the doublet. This should give an upper limit to any potential overestimation of the stability of high-spin species. In addition, the change in total charge of the system gives additional uncertainties with respect to the environmental effects. Therefore, it cannot be excluded that the relative stability of Co^{III}-H is underestimated in the current calculations and that it still is responsible for the oxidation wave in the experimental CV, possibly after rebinding a Cl^- ligand as discussed below.

Still, the potential Co^{III}-H intermediate is not the catalytically species because the most important factor favoring the Co^{II}-H pathway is the difference in barriers relative to the preceding hydrides, 8.7 kcal mol^{-1} for Co^{II}-H (**TS2′**) compared to 26.3 kcal mol^{-1} for Co^{III}-H (**TS1**). As each barrier is both calculated with reactants and TS of the same charge and spin multiplicity, the relative barrier heights are not expected to show significant method sensitivity. In a computational study of a cobalt(diimine–dioxime) complex, Artero and co-workers showed that there is a more favorable electrostatic interaction between the hydride and the water proton in the reduced species [29]. This is also the case for this Co-bpma complex. Looking at the charge distribution of the Co-H species, only Co^{II}-H can be convincingly described as a hydride. The NBO charge populations

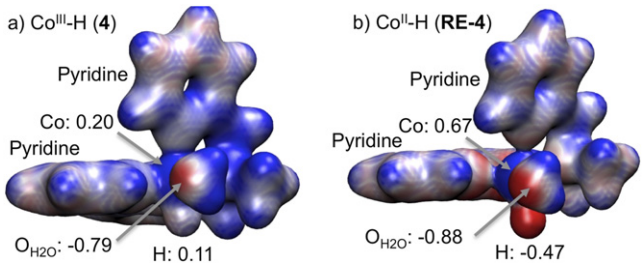

Figure 8. Electrostatic potentials and selected NBO charge populations of (a) Co^{III}-H (**4**) and (b) Co^{II}-H (**RE-4**). Blue denotes a more positive potential and red a more negative potential. Due to the difference in total charge between the two complexes, +2 and +1 respectively, the electrostatic potential is plotted using different intervals, 0.25–0.45 for Co^{III}-H and 0.1–0.3 for Co^{III}-H.

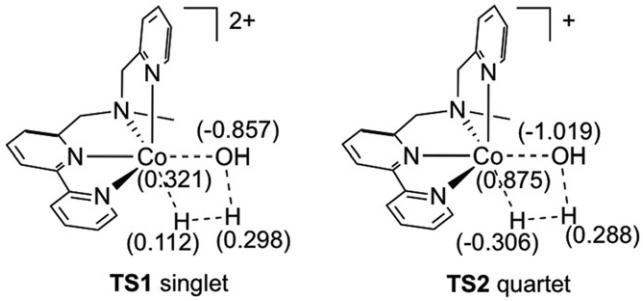

Figure 9. NBO charge populations (in parenthesis) in TS for the hydrogen formation from cobalt-hydride and water. **TS1** corresponds to Co^{III}-H and **TS2′** to Co^{II}-H.

on the hydrogen is negative (−0.47) and the electrostatic potential in that region is more negative than other parts of the complex, with the exception of the oxygen of the water ligand, see figure 8. In Co^{III}-H, the charge population of the hydrogen is instead positive (0.11), which is also reflected in the electrostatic potential.

The differences in charge distribution between the two hydrides are also seen in the corresponding TS. The charge is around 0.3 for the water proton, while the charge of the hydride in the TS is 0.11 in Co^{III}-H (**TS1**) and −0.31 in Co^{II}-H (**TS2′**), see figure 9. The latter TS is thus favored from an electrostatic perspective, because it represents hydrogen formation between a negative hydride and a positive proton. In addition to the higher stability of Co^{II}-H and the more favorable electrostatic interactions in the TS, this path is also favored by the higher stability of the product species Co^{II}-OH (**6**) compared to Co^{III}-OH (**5**), see figures 4 and 5.

These electrostatic considerations can also be used to argue against bimolecular mechanism involving two cobalt-hydride species. A reaction between two Co^{II}-H species would occur between negatively charged hydrides, which would be electrostatically unfavorable compared to a hydride–proton reaction. A reaction between two Co^{III}-H complexes would also miss the electrostatic stabilization expected for hydride–proton reactions.

4.2. Comparing hydride–water and hydride–ligand pathways

Of the different reaction pathways, the two pathways **b** and **d** have similar low barriers for hydrogen evolution. To facilitate comparison, the different stationary points for the complex with water bound in the second open ligand site are shown together in figure 10. Both pathways start with reduction of Co^{II} to Co^{I}. This step should correspond to the reduction wave at −1.4 V in the experimental CV [52]. The calculated reduction potential varies slightly depending on the identity of the ligands in the two exchangeable sites, but is in good agreement with experiment. From Co^{I}, a PCET process leading to Co^{II}-H (**RE-4**) occurs at a similar potential as the preceding reduction.

After the formation of Co^{II}-H (**RE-4**), the pathways diverge, see figure 11. H–H bond formation with a water ligand (**TS2′**) has a barrier of 9.3 kcal mol^{-1} relative to [Co^{II}(bpma)(H$_2$O)$_2$] (**2**), while the reaction with a protonated ligand (**TS6**) has a barrier of 9.4 kcal mol^{-1}. The similarity in barrier heights suggests that both routes should be possible. The presence of two open coordination sites in cis position for the Co-bpma complex thus gives two possible routes to hydrogen formation.

To evaluate the reliability of the two barrier heights, it is important to consider that from the [Co^{II}(bpma)(H$_2$O)$_2$] (**2**) starting point, two electrons and only one proton is required to reach Co^{II}-H (**RE-4**) and the proceeding transition state (**TS2′**). In comparison, Co^{II}-H(NH) **RE-8** and **TS6** requires the addition

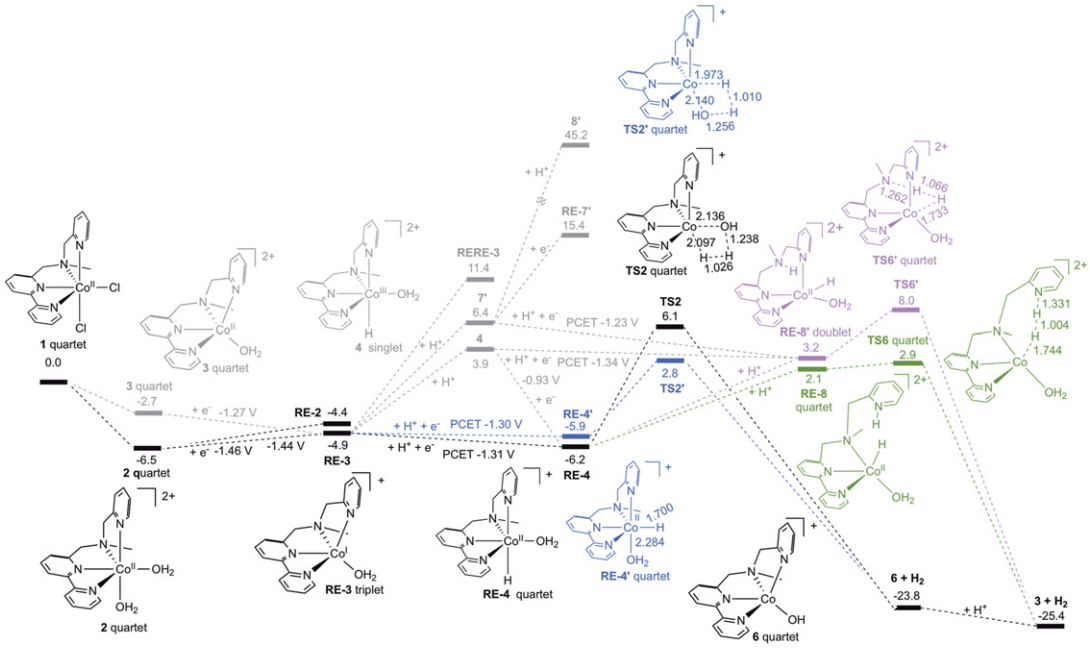

Figure 10. Summary of reaction pathways with a water ligand. Relative free energies are given in kcal mol^{-1} with [Co^{II}(bpma)Cl$_2$] as reference. Selected bond distances are given in Å.

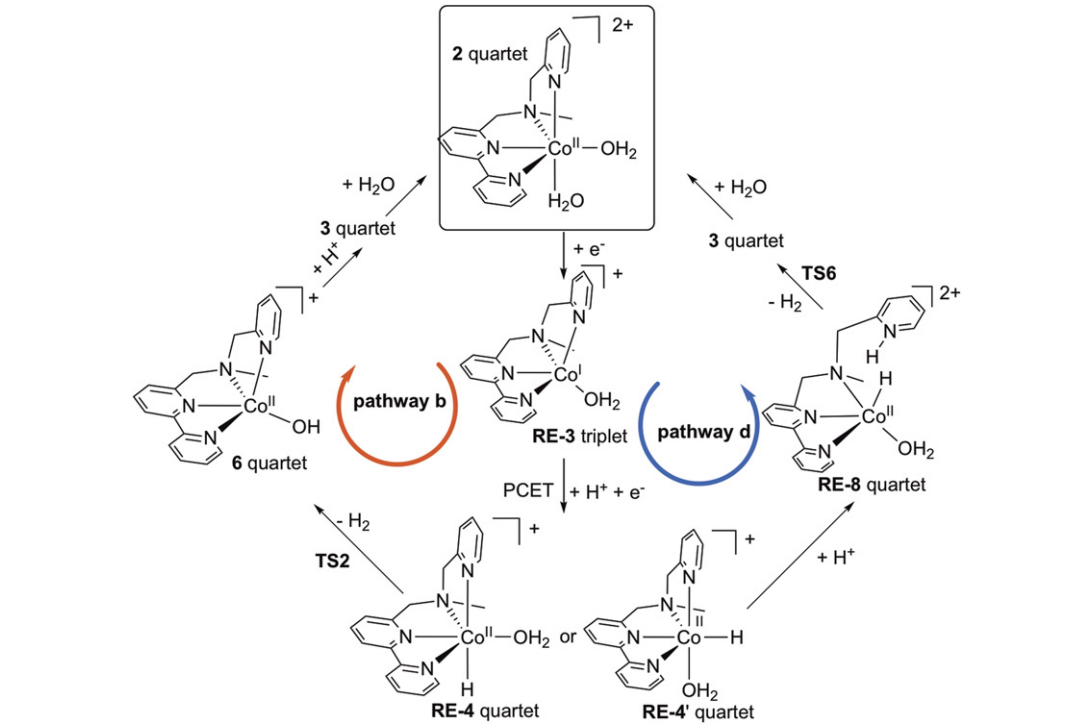

Figure 11. Comparison of the reaction mechanism for proton reduction by cobalt complex [Co^{II}(bpma)(H$_2$O)]$^{2+}$ through pathways **b** and **d**.

of two electrons and two protons. The difference in charge between the two TS leads to significant environmental effects on the relative barrier heights. Although it is clear that both pathways present viable reaction mechanisms, it is difficult to computationally pinpoint the relative importance of the two pathways.

4.3. pH dependence of key reaction steps

The computational results showing initial reduction of Co^{II} to Co^{I} around 1.4 eV, followed by a PCET process leading to Co^{II}-H (**RE-4**) at a similar potential are consistent with the pH dependence of the reduction wave

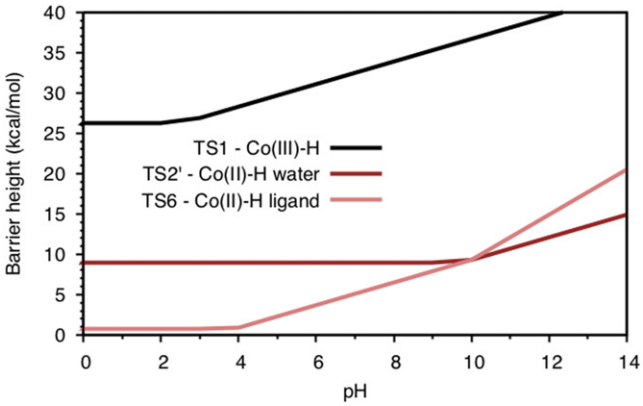

Figure 12. Calculated pH dependence of the key reaction barriers **TS1** (pathway **a**), **TS2′** (pathway b) and **TS6** (pathway d).

in the experimental CV, which shows a catalytic reaction at low pH that becomes reversible at high pH [52]. Figure SI-11 shows how the potentials of the steps leading to Co^{II}-H formation changes with pH. At higher pH, the PCET step becomes unfavorable, which prevents the formation of the hydride. The reaction then stops at the Co^{I} species and the oxidation wave reverts Co^{I} back to Co^{II}.

Changing the pH also affects the calculated barrier heights of the different reaction routes, see figure 12. The hydride–water pathway (**b**) shows a pH dependence if the potential of the PCET step leading to Co^{II}-H formation is close to that of the first Co^{II}/Co^{I} reduction, which is the case for high pH values. The hydride–ligand mechanism has the same pH dependence for Co^{II}-H generation, and also has a ligand protonation step for which the reaction energy is directly dependent on the pH. It thus shows two different pH behaviors, with a second-order pH-dependence at higher pH.

Comparing the reaction barriers of the two Co^{II}-H routes shows that at lower pH, the ligand donor mechanism becomes more favorable than the water donor mechanism. This can be explained by a decrease in the cost of protonating the ligand, which coupled with a low intrinsic barrier leads to a dominating contribution from that channel. The Co^{III}-H route remains significantly higher in energy for all pH values.

4.4. Effects of the second exchangeable coordination site

The presence of two exchangeable coordination sites not only opens up pathways that directly involve both sites, but a spectator ligand introduces an additional dimension in the other pathways. Instead of assuming a complete exchange of ligands, the full reaction pathways have been calculated with different ligand configurations, thus accounting for changes in relative ligand affinity during the reaction. The barrier for the reaction between Co^{II}-H and the protonated bpma ligand, pathway **d**, is affected by the identity of the spectator ligand. With Cl^{-}, the barrier for **TS6-Cl** relative to **2-Cl** is 7.1 kcal mol^{-1}, see figure 7, which can be compared to 9.4 kcal mol^{-1} with H_2O (**TS6** relative to **2**, see figure 6). If instead the coordination site is vacant, the barrier is higher (13.3 kcal mol^{-1}, see figure SI-9).

The calculated energy differences for different ligand binding alternatives are small. There are also considerable uncertainties associated with these calculations because of the changes in total system charge when adding or removing Cl^{-} ligands. Still, the reaction sequence with ligand exchange in Co^{II} and loss of water after reduction to Co^{I}, is in agreement with detailed studies of the early reaction steps [14, 38, 62]. Even if there is no Cl^{-} bound in Co^{I} (**3**) the binding affinity increases after protonation. For a potential Co^{III}-H species, Cl^{-} binding becomes favorable by a small margin (1.6 kcal mol^{-1}) compared to binding water (**4-Cl** and **4**). The different pathways with Cl^{-} bound are shown in figure SI-10, which can be compared to figure 10 for water. Further, with a negative Cl^{-}, the stability of Co^{III}-H (**4-Cl**) increases significantly relative to Co^{II}-H (**RE-4-Cl**). It is still predicted to be less stable than Co^{I} (**3-Cl**), but it would only be 2.1 kcal mol^{-1} less stable than Co^{II}-H. This is well within the error margin of the calculations. The assigned Co^{III}-H intermediate in the CV could thus come from a Cl-bound species.

Going further along the reaction pathway, reduction to Co^{II}-H intermediate (**RE-4**) again leads to lower affinity for Cl^{-}, and pathway **b** that requires a water ligand can still proceed. However, for pathway **d**, a subsequent protonation to Co^{II}-H(NH) (**RE-8**) is favored by the presence of the negative charge. This gives a relative stabilization of the doubly protonated species by 2.0 kcal mol^{-1}, see figures 6 and 7. From here, the barrier height is similar in the two pathways, which in total leads to a lower barrier with Cl^{-}. Considering the small energy differences, the real effect of the spectator ligand will depend on the complex and the ligand

exchange kinetics, but the results show the need to consider different binding modes, beyond characterization of the early Co^{II} and Co^{I} intermediates.

The mechanism with Cl^- bound is also relevant for the modeling of H_2 evolution from $[Co^{II}(bpma)Cl_2]$ in CH_3CN in the presence of excess protons [52]. Under these conditions, only the hydride–ligand pathway **d** is available, with the exception of reactions directly between cobalt-hydride and acid. The low reaction barrier for pathway **d** is not expected to change significantly when going between CH_3CN to water solvent and should therefore be considered as a possible mechanism also under acidic conditions.

Another possibility would be that the coordination site remains vacant beyond Co^{I}. The energy of such a Co^{II}-H intermediate (**RE-4-v**) is only 1.6 kcal mol^{-1} higher than with water (**RE-4**), see figure 10 and figure SI-9. However, from here bpma ligand protonation is more unfavorable, which in turn contributes to the higher total barrier. Based on these results, the cobalt ligands that participate in σ and π donation increase the proton affinity of the cobalt-hydride, which leads to lower TS barriers for hydrogen formation.

4.5. The impact of mechanistic variations

The calculations further illustrate the complexity of the reaction pathways through variations in bpma ligand protonation sites, isomers, and spin multiplicities. Starting with the protonation site, pyridyl protonation gives more favorable reaction barriers than amine protonation with both H_2O (**TS6/TS6′**) and Cl^- ligands (**TS6-Cl/TS6-Cl′**), see figure 10 and figure SI-10. This seems partly due to favorable steric interactions for H–H bond formation because the preference for pyridyl protonation increases when approaching the TS. If instead the sixth site is vacant, the amine pathway (**TS6-v′**) is slightly favored, see figure SI-9. The coupling between coordination environment and the protonation site, and the fact that stabilities change during the reaction, illustrates the importance of exploring multiple protonation sites.

For complexes with two exchangeable sites in cis position, different isomers must also be considered. For the hydride–water pathway (**b**), the axial hydride isomer of Co^{II}-H (**RE-4**) is slightly more stable than the equatorial one (**RE-4′**). However, when approaching the TS the equatorial hydride (**TS2′**) is favored by more than 3 kcal mol^{-1}, see figure 5.

The last dimension that has been explored is the spin multiplicity. Considering the small energy differences between different spin multiplicities relative to the functional sensitivity, a comparison of pathways should include all relevant potential energy surfaces. In general, the starting Co^{II} structures (**1/2**) are d^7 quartets, the reduced Co^{I} (**3**) are d^8 triplets, Co^{III}-H (**4**) are d^6 singlets, while Co^{II}-H (**RE-4**) are d^7 quartets, see table SI-3. The hydride–water pathway (**TS2′**) also stays on the quartet potential energy surface, see figure 5. The situation is more interesting for the hydride–ligand pathway **d**. The amine-protonated Co^{II}-H(NH) structures (**RE-8′**) are predicted to be doublets that would go through spin transitions to quartets during the H–H bond formation reactions (**TS6′**), see figures SI-7–SI-9.

Finally, the differences between protonation sites, isomers and spin multiplicities are all significant compared to the energy differences between the proposed pathways **b** and **d**, showing the relative importance of all these variations when modeling the reactivity of the Co-bpma catalyst.

5. Conclusion

The modeling of the tetradentate polypyridyl complex $[Co^{II}(bpma)Cl_2]$ with two open coordination sites in cis position clearly shows how these sites open up new mechanistic possibilities. Proton reduction can occur through two different pathways, both involving a Co^{II}-H intermediate. Co^{II}-H is favored over Co^{III}-H because only the former is a negative hydride that can react with a positive proton with a low barrier.

The first pathway where H–H bond formation occurs between the hydride and a water ligand requires both cis sites and is unique for these types of complexes. The second pathway involves protonation of the bpma ligand, which is similar to the proposed mechanism for pentadentate ligands. One of the cis sites then acts as spectator. The binding affinity of this site changes significantly during the reaction, which opens up the possibility that a negative ligand like Cl^- stabilizes the formation of a Co^{III}-H intermediate observed in the CV, as well as the doubly protonated $Co^{II}H(LH)$ intermediate that leads directly to formation of H_2. To properly explore the potential reaction mechanisms of the Co-bpma complex requires consideration of different protonation sites, isomers and spin multiplicities, and their combinations, leading to a large number of possibilities. In the ligand protonation pathway, the lowest barrier is obtained for a protonated pyridyl with the hydride in the same equatorial plane, even though that isomer is not stable in the preceding intermediate. This, together with the changes in binding affinity in the open ligand site, shows the importance of following different variations through the full reaction pathway of this class of cobalt catalysts.

Conflict of interest statement

There are no conflicts of interest to declare.

Funding

The authors acknowledge financial support from the Department of Chemistry—Ångström Laboratory, Uppsala University. The computations were enabled by resources in project Swedish National Infrastructure for Computing (SNIC) 2021/5-474 provided by the SNIC at NSC Tetralith, partially funded by the Swedish Research Council through Grant Agreement No. 2018-05973.

Data availability statement

All data that support the findings of this study are included within the article (and any supplementary files).

ORCID iDs

Sofia Kiriakidi https://orcid.org/0000-0003-2509-3277
Anders Thapper https://orcid.org/0000-0001-7643-302X
Sascha Ott https://orcid.org/0000-0002-1691-729X
Marcus Lundberg https://orcid.org/0000-0002-1312-1202

References

[1] Du P and Eisenberg R 2012 *Energy Environ. Sci.* **5** 6012–21
[2] Artero V and Fontecave M 2013 *Chem. Soc. Rev.* **42** 2338–56
[3] Wang M, Na Y, Gorlov M and Sun L 2009 *Dalton Trans.* **33** 6458–67
[4] Wang F, Wang W-G, Wang H-Y, Si G, Tung C-H and Wu L-Z 2012 *ACS Catal.* **2** 407–16
[5] Zee D Z, Chantarojsiri T, Long J R and Chang C J 2015 *Acc. Chem. Res.* **48** 2027–36
[6] Ran J, Zhang J, Yu J, Jaroniec M and Qiao S Z 2014 *Chem. Soc. Rev.* **43** 7787–812
[7] Mazzeo A, Santalla S, Gaviglio C, Doctorovich F and Pellegrino J 2021 *Inorg. Chim. Acta* **517** 119950
[8] Bauer E B 2015 Iron catalysis: historic overview and current trends *Iron Catalysis II* (Berlin: Springer) pp 1–18
[9] McCrory C C L, Uyeda C and Peters J C 2012 *J. Am. Chem. Soc.* **134** 3164–70
[10] Losse S, Vos J G and Rau S 2010 *Coord. Chem. Rev.* **254** 2492–504
[11] Queyriaux N, Jane R T, Massin J, Artero V and Chavarot-Kerlidou M 2015 *Coord. Chem. Rev.* **304–305** 3–19
[12] Tong L, Zong R and Thummel R P 2014 *J. Am. Chem. Soc.* **136** 4881–4
[13] Sun Y, Sun J, Long J R, Yang P and Chang C J 2013 *Chem. Sci.* **4** 118–24
[14] King A E, Surendranath Y, Piro N A, Bigi J P, Long J R and Chang C J 2013 *Chem. Sci.* **4** 1578–87
[15] Hoffert W A, Roberts J A S, Morris Bullock R and Helm M L 2013 *Chem. Commun.* **49** 7767–9
[16] Yang Y, Wang M, Xue L, Zhang F, Chen L, Ahlquist M S G and Sun L 2014 *ChemSusChem* **7** 2889–97
[17] Tong L, Duan L, Zhou A and Thummel R P 2020 *Coord. Chem. Rev.* **402** 213079
[18] Chen X, Ren H, Peng W, Zhang H, Lu J and Zhuang L 2014 *J. Phys. Chem* C **118** 20791–8
[19] Roy S, Huang Z, Bhunia A, Castner A, Gupta A K, Zou X and Ott S 2019 *J. Am. Chem. Soc.* **141** 15942–50
[20] Gottschling K, Savasci G, Vignolo-González H, Schmidt S, Mauker P, Banerjee T, Rovó P, Ochsenfeld C and Lotsch B V 2020 *J. Am. Chem. Soc.* **142** 12146–56
[21] Lewandowska-Andralojc A, Malolepszy A, Stritt A and Grohmann A 2020 *Catal. Sci. Technol.* **10** 4693–702
[22] Benazzi E, Begato F, Niorettini A, Destro L, Wurst K, Licini G, Agnoli S, Zonta C and Natali M 2021 *J. Mater. Chem.* A **9** 20032–9
[23] Smith P T, Benke B P, An L, Kim Y, Kim K and Chang C J 2021 *ChemElectroChem* **8** 1653–7
[24] Schrauzer G N and Holland R J 1971 *J. Am. Chem. Soc.* **93** 1505–6
[25] Dempsey J L, Winkler J R and Gray H B 2010 *J. Am. Chem. Soc.* **132** 16774–6
[26] Stubbert B D, Peters J C and Gray H B 2011 *J. Am. Chem. Soc.* **133** 18070–3
[27] Valdez C N, Dempsey J L, Brunschwig B S, Winkler J R and Gray H B 2012 *Proc. Natl Acad. Sci.* **109** 15589–93
[28] Jacques P-A, Artero V, Pécaut J and Fontecave M 2009 *Proc. Natl Acad. Sci. USA* **106** 20627–32
[29] Bhattacharjee A, Andreiadis E S, Chavarot-Kerlidou M, Fontecave M, Field M J and Artero V 2013 *Chem. Eur. J.* **19** 15166–74
[30] Jiang Y-K and Liu J-H 2012 *Int. J. Quantum Chem.* **112** 2541–6
[31] Muckerman J T and Fujita E 2011 *Chem. Commun.* **47** 12456–8
[32] Solis B H and Hammes-Schiffer S 2011 *J. Am. Chem. Soc.* **133** 19036–9
[33] Dempsey J L, Brunschwig B S, Winkler J R and Gray H B 2009 *Acc. Chem. Res.* **42** 1995–2004
[34] Artero V, Chavarot-Kerlidou M and Fontecave M 2011 *Angew. Chem., Int. Ed.* **50** 7238–66
[35] Kaeffer N, Chavarot-Kerlidou M and Artero V 2015 *Acc. Chem. Res.* **48** 1286–95
[36] Krishnan C V and Sutin N 1981 *J. Am. Chem. Soc.* **103** 2141–2
[37] Creutz C and Sutin N 1985 *Coord. Chem. Rev.* **64** 321–41
[38] Li Z-J *et al* 2016 *J. Phys. Chem. Lett.* **7** 5253–8
[39] Liu J, Liao R-Z, Heinemann F W, Meyer K, Thummel R P, Zhang Y and Tong L 2021 *Inorg. Chem.* **60** 17976–85
[40] Lucarini F *et al* 2021 *ChemSusChem* **14** 1874–85
[41] Bigi J P, Hanna T E, Harman W H, Chang A and Chang C J 2010 *Chem. Commun.* **46** 958–60

[42] Sun Y, Bigi J P, Piro N A, Tang M L, Long J R and Chang C J 2011 *J. Am. Chem. Soc.* **133** 9212–5
[43] Singh W M *et al* 2012 *Angew. Chem., Int. Ed.* **51** 5941–4
[44] Zhang P, Wang M, Gloaguen F, Chen L, Quentel F and Sun L 2013 *Chem. Commun.* **49** 9455–7
[45] Khnayzer R S, Thoi V S, Nippe M, King A E, Jurss J W, El Roz K A, Long J R, Chang C J and Castellano F N 2014 *Energy Environ. Sci.* **7** 1477–88
[46] Nippe M, Khnayzer R S, Panetier J A, Zee D Z, Olaiya B S, Head-Gordon M, Chang C J, Castellano F N and Long J R 2013 *Chem. Sci.* **4** 3934–45
[47] Shan B, Baine T, Ma X A N, Zhao X and Schmehl R H 2013 *Inorg. Chem.* **52** 4853–9
[48] Call A, Codolà Z, Acuña-Parés F and Lloret-Fillol J 2014 *Chem. Eur. J.* **20** 6171–83
[49] Bachmann C, Guttentag M, Spingler B and Alberto R 2013 *Inorg. Chem.* **52** 6055–61
[50] Deponti E, Luisa A, Natali M, Iengo E and Scandola F 2014 *Dalton Trans.* **43** 16345–53
[51] Zhao X, Wang P and Long M 2017 *Comments Inorg. Chem.* **37** 238–70
[52] Singh W M, Mirmohades M, Jane R T, White T A, Hammarström L, Thapper A, Lomoth R and Ott S 2013 *Chem. Commun.* **49** 8638–40
[53] Guttentag M, Rodenberg A, Bachmann C, Senn A, Hamm P and Alberto R 2013 *Dalton Trans.* **42** 334–7
[54] Rodenberg A, Orazietti M, Probst B, Bachmann C, Alberto R, Baldridge K K and Hamm P 2014 *Inorg. Chem.* **54** 646–57
[55] Schnidrig S *et al* 2017 *ChemSusChem* **10** 4570–80
[56] Tang L-Z, Xue D, Yang L-F and Zhan S-Z 2017 *Transit. Met. Chem.* **42** 711–7
[57] Luo S-P, Tang L-Z and Zhan S-Z 2017 *Inorg. Chem. Commun.* **86** 276–80
[58] Lei J-M, Luo S-P and Zhan S-Z 2018 *Polyhedron* **154** 295–301
[59] Call A, Franco F, Kandoth N, Fernández S, González-Béjar M, Pérez-Prieto J, Luis J M and Lloret-Fillol J 2018 *Chem. Sci.* **9** 2609–19
[60] Vennampalli M, Liang G, Katta L, Webster C E and Zhao X 2014 *Inorg. Chem.* **53** 10094–100
[61] Wang P *et al* 2018 *J. Am. Chem. Soc.* **140** 9219–29
[62] Wang P, Liang G, Webster C E and Zhao X 2020 *Eur. J. Inorg. Chem.* **2020** 3534–47
[63] Guo X, Li C, Wang W, Zhang B, Hou Y, Wang X and Zhou Q 2021 *RSC Adv.* **11** 24359–65
[64] Guo X, Li C, Wang W, Hou Y, Zhang B, Wang X and Zhou Q 2021 *Dalton Trans.* **50** 2042–9
[65] Forsberg J, Grasjo J, Brena B, Nordgren J, Duda L C and Rubensson J E 2009 *Phys. Rev.* B **79** 132203
[66] Wang P, Liang G, Boyd C L, Webster C E and Zhao X 2019 *Eur. J. Inorg. Chem.* **2019** 2134–9
[67] Lubitz W, Ogata H, Rüdiger O and Reijerse E 2014 *Chem. Rev.* **114** 4081–148
[68] Yang X and Hall M B 2009 *J. Am. Chem. Soc.* **131** 10901–8
[69] Camara J M and Rauchfuss T B 2012 *Nat. Chem.* **4** 26
[70] Schilter D, Camara J M, Huynh M T, Hammes-Schiffer S and Rauchfuss T B 2016 *Chem. Rev.* **116** 8693–749
[71] Ginovska-Pangovska B, Dutta A, Reback M L, Linehan J C and Shaw W J 2014 *Acc. Chem. Res.* **47** 2621–30
[72] Marinescu S C, Winkler J R and Gray H B 2012 *Proc. Natl Acad. Sci. USA* **109** 15127–31
[73] Lewandowska-Andralojc A, Baine T, Zhao X, Muckerman J T, Fujita E and Polyansky D E 2015 *Inorg. Chem.* **54** 4310–21
[74] Wiedner E S and Bullock R M 2016 *J. Am. Chem. Soc.* **138** 8309–18
[75] Tong L, Kopecky A, Zong R, Gagnon K J, Ahlquist M S G and Thummel R P 2015 *Inorg. Chem.* **54** 7873–84
[76] Panneerselvam M and Jaccob M 2018 *Inorg. Chem.* **57** 8116–27
[77] Becke A D 1993 *J. Chem. Phys.* **98** 5648–52
[78] Grimme S, Antony J, Ehrlich S and Krieg H 2010 *J. Chem. Phys.* **132** 154104
[79] Reiher M, Salomon O and Artur Hess B 2001 *Theor. Chem. Acc.* **107** 48–55
[80] Siegbahn P E M, Blomberg M R A and Chen S-L 2010 *J. Chem. Theory Comput.* **6** 2040–4
[81] Boniolo M *et al* 2021 *Dalton Trans.* **50** 660–74
[82] Frisch M J *et al* 2009 *Gaussian09, Revsion D.01* (Wallingford, CT)
[83] Marenich A V, Cramer C J and Truhlar D G 2009 *J. Phys. Chem.* B **113** 6378–96
[84] Dunning T H Jr 1989 *J. Chem. Phys.* **90** 1007–23
[85] Fukui K 1981 *Acc. Chem. Res.* **14** 363–8
[86] Poli R and Harvey J N 2003 *Chem. Soc. Rev.* **32** 1–8
[87] Lundberg M and Siegbahn P E M 2005 *Chem. Phys. Lett.* **401** 347–51
[88] Kendall R A, Dunning T H Jr and Harrison R J 1992 *J. Chem. Phys.* **96** 6796–806
[89] Tissandier M D, Cowen K A, Feng W Y, Gundlach E, Cohen M H, Earhart A D, Coe J V and Tuttle T R 1998 *J. Phys. Chem.* A **102** 7787–94
[90] Keith J A and Carter E A 2012 *J. Chem. Theory Comput.* **8** 3187–206
[91] McQuarrie D A 2000 *Statistical Mechanics* 2nd edn (Mill Valley, CA: University Science Books)
[92] Greeley R S, Smith W T Jr, Stoughton R W and Lietzke M H 1960 *J. Phys. Chem.* **64** 652–7
[93] Isse A A and Gennaro A 2010 *J. Phys. Chem.* B **114** 7894–9
[94] Li J, Fisher C L, Chen J L, Bashford D and Noodleman L 1996 *Inorg. Chem.* **35** 4694–702
[95] Gilson R and Durrant M C 2009 *Dalton Trans.* **46** 10223–30
[96] Jerome S V, Hughes T F and Friesner R A 2014 *J. Phys. Chem.* B **118** 8008–16
[97] Baik M-H and Friesner R A 2002 *J. Phys. Chem.* A **106** 7407–12
[98] Roy L E, Batista E R and Hay P J 2008 *Inorg. Chem.* **47** 9228–37
[99] Glendening E D, Reed A E, Carpenter J E and Weinhold F 1998 *NBO Version 3.1* (Madison, WI: University of Wisconsin Press)
[100] Wiberg K B 1968 *Tetrahedron* **24** 1083–96
[101] Lo W K C *et al* 2016 *Inorg. Chem.* **55** 4564–81
[102] Fogeron T, Porcher J-P, Gomez-Mingot M, Todorova T K, Chamoreau L-M, Mellot-Draznieks C, Li Y and Fontecave M 2016 *Dalton Trans.* **45** 14754–63
[103] Panetier J A, Letko C S, Tilley T D and Head-Gordon M 2015 *J. Chem. Theory Comput.* **12** 223–30